Computer simulations of vapour-liquid phase equilibria of n-alkanes.

Smit, B.; Karaborni, S.; Siepmann, J.I.

DOI
10.1063/1.469563
Publication date
1995

Published in
Journal of Chemical Physics

Computer simulations of vapor–liquid phase equilibria of *n*-alkanes

Berend Smit,[a] Sami Karaborni, and J. Ilja Siepmann[b]
Shell Research B.V., Koninklijke/Shell-Laboratorium, Amsterdam, P.O. Box 38000, 1030 BN Amsterdam, The Netherlands

(Received 1 April 1994; accepted 25 October 1994)

For petrochemical applications knowledge of the critical properties of the *n*-alkanes is of interest even at temperatures where these molecules are thermally unstable. Computer simulations can determine the vapor–liquid coexistence curve of a large number of *n*-alkanes ranging from pentane (C_5) through octatetracontane (C_{48}). We have compared the predicted phase diagrams of various models with experimental data. Models which give nearly identical properties of liquid alkanes at standard conditions may have critical temperatures that differ by more than 100 K. A new *n*-alkane model has been developed by us that gives a good description of the phase behavior over a large temperature range. For modeling vapor–liquid coexistence a relatively simple united atom model was sufficient to obtain a very good agreement with experimental data; thus it appears not necessary to take the hydrogen atoms explicitly into account. The model developed in this work has been used to determine the critical properties of the long-chain alkanes for which experiments turned out to be difficult and contradictory. We found that for the long-chain alkanes (C_8–C_{48}) the critical density decreases as a function of the carbon number. These simulations were made possible by the use of a recently developed simulation technique, which is a combination of the Gibbs-ensemble technique and the configurational-bias Monte Carlo method. Compared with the conventional Gibbs-ensemble technique, this method is several orders of magnitude more efficient for pentane and up to a hundred orders of magnitude for octatetracontane. This recent development makes it possible to perform routinely phase equilibrium calculations of complex molecules. © *1995 American Institute of Physics.*

I. INTRODUCTION

Anyone who has tried to construct an igloo in the desert can testify to the importance of elementary knowledge of phase behavior. Besides being of practical interest, phase equilibria have been the topic of many fundamental studies since the seminal work of van der Waals. Since knowledge of the phase behavior is essential in many practical applications, there have been significant experimental efforts towards the determination of unknown or partially known phase diagrams.

It is interesting to note that in the work of van der Waals a connection has already been made between the intermolecular potential and the phase behavior of the molecules. To determine the phase diagram of a given model proved to be an extremely difficult task. Exact analytical solutions have been obtained for only a few important but exceptional cases. For exact data for a given model one therefore has to rely on the results of computer simulations. The calculation of a phase diagram via computer simulations used to be an elaborate task which required many simulations.[1] An important step forward was the development of the Gibbs-ensemble technique by Panagiotopoulos.[2–4] By this method data on phase coexistence can be obtained from one single simulation. The Gibbs-ensemble technique has been applied successfully to determine the vapor–liquid and liquid–liquid coexistence curves of various model fluids. Panagiotopoulos[5] recently reviewed the applications of the Gibbs-ensemble technique.

One of the Monte Carlo steps in the Gibbs-ensemble technique is the transfer of molecules between the liquid phase and gas phase. For chain molecules, this step results in a prohibitively low acceptance of transfers from the gas phase into the liquid phase. Therefore the Gibbs ensemble used to be limited to systems containing atoms or small molecules. Recently, the Gibbs-ensemble technique has been combined with the configurational-bias Monte Carlo method.[6–8] Instead of a random insertion, in the configurational-bias Monte Carlo scheme molecules are grown atom by atom in such a way that regions of favorable energy are found and overlap with other molecules is avoided.[9–12] This growing scheme introduces a bias that can be removed exactly by adjusting the acceptance rules.[9,12] A similar approach has been used by Cracknell *et al.*[13] to perform Gibbs-ensemble simulations using a rotational-bias insertion of water molecules. The combination of the Gibbs-ensemble technique with the configurational-bias Monte Carlo method has been applied successfully to determine the vapor–liquid coexistence curve of chains of Lennard-Jones beads[6] and alkanes.[8,14,15]

The description of alkanes has received considerable interest. Many different models for these molecules have been proposed.[16–25,11] One of the first models for liquid butane was developed by Ryckaert and Bellemans.[17] This model assumes that every CH_3 or CH_2 group can be described as one single interaction site. The dispersive interactions of these ''united atoms'' are described by a Lennard-Jones potential. The bond lengths and bond angles are kept fixed. Changes in the dihedral angle are described with a torsion potential which has been fitted to yield the experimental distribution of *gauche/trans* conformers. This type of model

[a]Author for correspondence.
[b]Present address: Department of Chemistry, University of Minnesota, Minneapolis, Minnesota 55455.

 0021-9606/95/102(5)/2126/15/$6.00

was extended to longer chain lengths by Jorgensen and co-workers.[19,20] At high densities the assumption that the CH_3 and CH_2 groups can be modeled as united atoms tends to fail. Indeed simulations of alkane crystals[26,27] and dense monolayers of alkanes[28,29] show that united atom models do not describe the packing of alkane molecules correctly, and that it is important to take the hydrogen atoms explicitly into account. Because of the increased number of interaction sites, these ''all atoms models''[16] are much more demanding with regard to their use in a simulation. An interesting compromise between the united atom approach and the all atoms models is the use of anisotropic potentials as proposed by Toxvaerd.[21] The anisotropy is introduced to make the interaction between the CH_3 and CH_2 groups dependent on the conformation, i.e., the interaction is different when the CH_2 group points with its ''H-side'' or ''C-side'' towards another CH_2 group. Toxvaerd has shown that such an anisotropic model gives a better description of the equation of state of dense alkanes under high pressure than that of some of the isotropic models.[21]

Most of these alkane models have been fitted to liquid properties such as heats of vaporization and liquid densities at standard conditions. In this work, we address the question how accurately the phase behavior of *n*-alkanes can be modeled over a large range of temperatures and chain lengths.

The critical properties of the *n*-alkanes are of interest for petrochemical applications. We use the Gibbs-ensemble simulations to estimate the chain length dependence of these critical properties at conditions where experiments are not possible.

In Secs. II and III we describe the simulation techniques and in Sec. IV the models that have been studied in this work, as well as the results of the simulations. In Sec. V, we present the simulation results of the critical properties. Some preliminary results of this work have been described earlier.[14,15]

II. SIMULATION TECHNIQUES

In this section a description is given of the simulation techniques that are used in this work. A more extensive description of the Gibbs-ensemble technique[4,30] and the configurational-bias Monte Carlo method[11,12,31] can be found in the literature.

A. The Gibbs ensemble technique

Simulations in the Gibbs ensemble are performed using two boxes, each box having periodic boundary conditions. The boxes are kept at a constant temperature T, the total volume of the two boxes is fixed at V, and a fixed number of N particles are distributed over the two boxes. The two boxes are coupled via Monte Carlo rules that allow the exchange of particles and changes in the volume in such a way that the two boxes remain in thermodynamic equilibrium with each other.

The probability of finding a particular configuration in the Gibbs ensemble is given by[4,5,32]

$$\mathcal{N}(\beta,V_1,n_1;\xi^N) \propto \frac{V_1^{n_1}(V-V_1)^{N-n_1}}{(N-n_1)!\,n_1!} \times \exp[-\beta U_1(n_1)]\exp[-\beta U_2(N-n_1)], \quad (1)$$

where n_1 denotes the number of particles in box 1, V_1 the volume of box 1, ξ^N denotes the scaled (with respect to the box length) positions of the particles, and $U(n_i)$ is the intermolecular potential.

In a Gibbs-ensemble simulations the following Monte Carlo moves are used: displacement of particles in the boxes, changes in the volume, and exchange of particles between the two boxes. In the next section we use the configurational-bias Monte Carlo method for the exchange of particles. To introduce the notation, we consider the acceptance rules for this step in some detail. The derivations of the acceptance rules for the other moves are given elsewhere.[3,30]

Let us assume the system to be in a state o with n_1 particles in box 1 with volume V_1 and consider the move to the state n which has n_1+1 particles in box 1 with the same volume. The acceptance rule for this move is[3]

$$\mathrm{acc}(o\rightarrow n)=\min\left[1,\frac{V_1(N-n_1)}{(V-V_1)(n_1+1)} \times \exp\,(-\beta\Delta U_1)\,\exp\,(-\beta\Delta U_2)\right], \quad (2)$$

where $\Delta U_1 = U_1(n)-U_1(o)$ is defined as the energy difference in box 1 between state n and state o. This acceptance rule can be derived by imposing the condition of detailed balance

$$K(o\rightarrow n)=K(n\rightarrow o), \quad (3)$$

where $K(o\rightarrow n)$ is the flow of configurations from o to n. This flow of configurations is equal to the product of the probability of being in state o, the probability of generating state n and the probability of acceptance

$$K(o\rightarrow n)=\mathcal{N}(n_1,V_1;\xi^N)\times p(o\rightarrow n)\times \mathrm{acc}(o\rightarrow n). \quad (4)$$

For the reverse move, the removal of a particles from box 1, the flow is given by

$$K(n\rightarrow o)=\mathcal{N}(n_1+1,V_1;\xi^N)\times p(n\rightarrow o)\times \mathrm{acc}(n\rightarrow o). \quad (5)$$

Since it is decided at random whether to remove or insert a particle, we have $p(o\rightarrow n)=p(n\rightarrow o)$. Substitution of Eqs. (4) and (5) and distribution (1) together with the acceptance rule (2) shows that indeed detailed balance (3) is obeyed.

B. Configurational-bias Monte Carlo

In the conventional Gibbs-ensemble scheme particles are inserted at random positions. For a Lennard-Jones fluid the probability that an attempt to insert a particle in the liquid phase does not result in an overlap with one of the other liquid particles is of the order of 0.005.[33] At similar conditions, the probability that a chain of n atoms is successfully inserted will be of the order of 0.005^n. As a consequence the number of attempts to insert a particle increases enormously

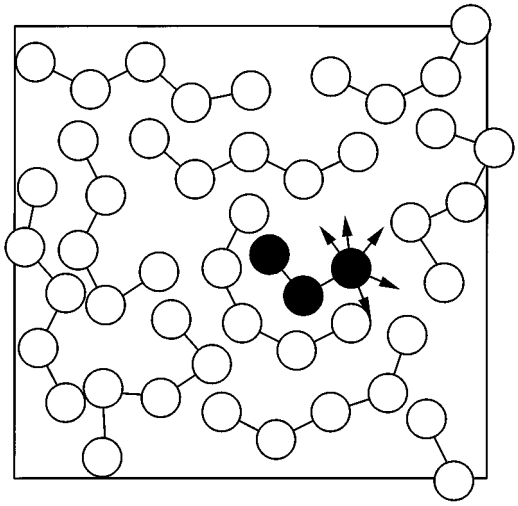

FIG. 1. Insertion of a chain molecule; the arrows indicate the k trial orientations to insert the fourth atom.

for larger chain lengths. This limits the applicability of the Gibbs-ensemble technique in its original form to very short chain molecules.

The configurational-bias Monte Carlo technique has been developed to insert chain molecules in moderately dense systems.[10–12] Here we give a brief description of this method, a more extensive discussion is given else where.[11,12,31]

Let us divide the potential energy of an atom into two contributions;[12,34] (1) the internal energy $u^{\rm int}$ which includes parts of the intramolecular interactions, and (2) the external energy $u^{\rm ext}$ which contains the intermolecular interactions and those intramolecular interactions that are not part of the internal energy. The division is to some extent arbitrary and depends on the details of the model. Note that in some implementations of the configurational-bias Monte Carlo technique this division is not used.[11] In Sec. IV B 2 we make a detailed comparison of the advantages of using this separation.

Instead of a random insertion of a molecule, we use the following procedure to ''grow'' a molecule atom by atom;

(1) The first atom is inserted at a random position, and the energy $u_1(n)$ is calculated together with

$$w_1(n)=\exp[-\beta u_1(n)]. \tag{6}$$

(2) To insert the next atom l, k trial orientations are generated (see Fig. 1). The set of k trial orientations are denoted by $\{\mathbf{b}\}_k=\mathbf{b}_1,\ \mathbf{b}_2,...,\mathbf{b}_k$. These orientations are not generated at random, but with a probability which is a function of the internal energy

$$p_l^{\rm int}(\mathbf{b}_i)=\frac{\exp[-\beta u_l^{\rm int}(\mathbf{b}_i)]}{C}. \tag{7}$$

Of each of these trial orientations the *external* energy is calculated $[u_l^{\rm ext}(\mathbf{b}_i)]$ together with the factor

$$w_l(n)=\sum_{j=1}^{k}\exp[-\beta u_l^{\rm ext}(\mathbf{b}_j)]. \tag{8}$$

Out of these k trial positions, we select one with probability

$$p_l^{\rm ext}(\mathbf{b}_i)=\frac{\exp[-\beta u_l^{\rm ext}(\mathbf{b}_i)]}{w_l(n)}. \tag{9}$$

(3) Step 2 is repeated $M-1$ times until the entire molecule is grown and the Rosenbluth factor of the molecule can be calculated

$$W(n)=\prod_{l=1}^{M} w_l(n). \tag{10}$$

This algorithm biases the insertion of a molecule such that regions with favorable energy are found and overlap with other atoms is avoided. The probability that a particular conformation is generated is given by

$$\begin{aligned}P(n)&=\prod_{l=2}^{M} p_l^{\rm int}(n)p_l^{\rm ext}(n)\\&=\prod_{l=2}^{M}\frac{\exp\{-\beta[u_l^{\rm int}(n)+u_l^{\rm ext}(n)]\}}{Cw_l(n)}\\&=\frac{\exp[-\beta U(n)]}{C^{M-1}W(n)},\end{aligned} \tag{11}$$

where the total energy of the inserted molecule is

$$U=\sum_{l=1}^{M} u_l=\sum_{l=1}^{M} u_l^{\rm int}u_l^{\rm ext}. \tag{12}$$

To perform a move, we have to calculate the Rosenbluth factor of the old configuration. This is done via the following steps:

(1) A particle is selected at random;
(2) The energy of the first atom is determined $u_1(o)$ together with

$$w_1(o)=\exp[-\beta u_1(o)]. \tag{13}$$

(3) For the next atom, l, $k-1$ trial orientations are generated with a probability given by Eq. (7). These trial orientations together with the actual position of the atom l form the set $\{\mathbf{b}'\}_k$ (see Fig. 2) for which we determine the factor

$$w_l(o)=\sum_{j=1}^{k}\exp[-\beta u_l(\mathbf{b}_j')]. \tag{14}$$

(4) Step 2 is repeated $M-1$ times until we have retraced the entire chain and the Rosenbluth factor of the chain can be calculated

$$W(o)=\prod_{l=1}^{M} w_l(o). \tag{15}$$

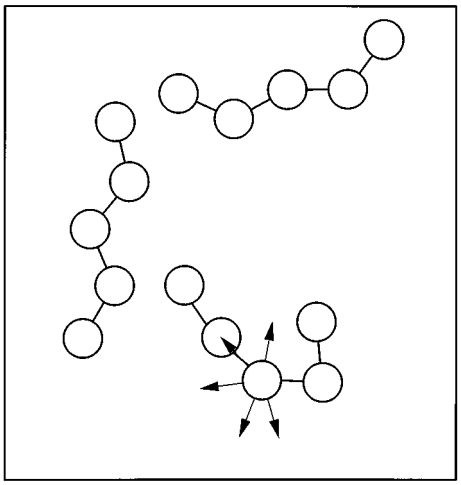

FIG. 2. Calculation of the Rosenbluth factor of the old conformation; the arrows give the set of directions for which the Rosenbluth factor of the second atom is calculated.

The above algorithms for the new and old configuration form the basis of the configurational-bias Monte Carlo technique. They need to be supplemented with acceptance rules that remove the bias from the insertion step. These acceptance rules depend on the type of move and type of ensemble. For example, in Refs. 10–12 acceptance rules are derived for a move in which part of the molecule is regrown.

C. Configurational-bias Monte Carlo and the Gibbs ensemble

In the Gibbs ensemble, we use the configurational-bias Monte Carlo technique to make the exchange of chain molecules between the two boxes possible.

Let us assume the system to be in state o with n_1 particles in box 1 with volume V_1 and we try to generate state n by moving a particle from box 2 into box 1. We use the algorithms of the previous section to grow a chain in box 1 and to calculate the Rosenbluth factor of the old conformation of the chain which is removed from box 2. We then accept this move with probability

$$\mathrm{acc}(o\rightarrow n)=\min\left[1,\frac{V_1(N-n_1)}{(V-V_1)(n_1+1)}\frac{W(n)}{W(o)}\right]. \tag{16}$$

We now have to demonstrate that this acceptance rule indeed removes the bias from the insertion step and hence the method indeed samples the correct distribution of configurations. As in Sec. II A, we impose the condition of detailed balance (3). The main difference is that in the configurational-bias Monte Carlo scheme the probability of generating a particular conformation does depend on the particular configuration of the molecules and the probability of generating the reverse move will be different. The probability of generating conformation n is given by [see Eq. (11)],

$$P(o\rightarrow n|\{\mathbf{b}\}_k)=\frac{\exp[-\beta U(n)]}{C^{M-1}W(n|\{\mathbf{b}\}_k)}. \tag{17}$$

For the reverse move, the insertion of a chain in box 2, we have

$$P(n\rightarrow o|\{\mathbf{b}'\}_k)=\frac{\exp[-\beta U(o)]}{C^{M-1}W(o|\{\mathbf{b}'\}_k)}. \tag{18}$$

Note that there are many different ways to generate a particular configuration n or o, namely all sets of trial orientations that include the selected orientation. Detailed balance implies that we have to sum over all of these. We can, however, impose a much stronger condition, super detailed balance, which states that for all sets of trial conformations individually detailed balance should be obeyed.[12] If super-detailed balance is obeyed, then detailed balance is certainly obeyed. By definition, for super-detailed balance we have to consider the same set of trial orientations for the moves $o\rightarrow n$ and $n\rightarrow o$, so

$$\begin{aligned}&\mathcal{N}(o)\times p(o\rightarrow n|\{\mathbf{b}\}_k,\{\mathbf{b}'\}_k)\times\mathrm{acc}(o\rightarrow n|\{\mathbf{b}\}_k,\{\mathbf{b}'\}_k)\\&\quad=\mathcal{N}(n)\times p(n\rightarrow o|\{\mathbf{b}'\}_k,\{\mathbf{b}\}_k)\\&\qquad\times\mathrm{acc}(n\rightarrow o|\{\mathbf{b}'\}_k,\{\mathbf{b}\}_k).\end{aligned} \tag{19}$$

Substitution of Eqs. (1), (17), and (18) gives as condition for the acceptance rule

$$\frac{\mathrm{acc}(o\rightarrow n|\{\mathbf{b}\}_k,\{\mathbf{b}'\}_k)}{\mathrm{acc}(n\rightarrow o|\{\mathbf{b}'\}_k,\{\mathbf{b}\}_k)}=\frac{V_1(N-n_1)}{(V-V_1)(n_1+1)}\frac{W(n)}{W(o)}. \tag{20}$$

Since acceptance rule (16) obeys this condition, we have demonstrated that the correct distribution is sampled.

We have outlined the general scheme of the Gibbs-ensemble technique combined with configurational-bias Monte Carlo. For a given model it is important to tune the technique optimally as will be discussed in the next sections.

III. DESCRIPTION OF THE SIMULATIONS

The simulations have been performed in cycles. Each cycle consists of R randomly selected Monte Carlo moves (we usually take R equal to the total number of molecules).[35] The type of moves we perform are (1) displacement of a randomly selected particle; (2) rotation of a randomly selected particle around the middle atom; (3) regrowing of parts of a randomly selected molecule; (4) change of volume of the two boxes; and (5) exchange of particles between the two boxes. The relative probability that a particular move is attempted is set to $p_1:p_2:p_3:p_4:p_5=0.222:0.222:0.222:0.006:0.328$. At low temperatures and for long chain alkanes the relative probability of attempting an exchange of particles was increased to ensure a sufficient number of successful exchanges.

Note that moves (1) and (2) do not change the internal structure of the molecule. In these moves the maximum displacement and maximum rotation are adjusted in such a way that 50% of the moves are accepted.

For move (3), the partial regrowing of a molecule, we select a molecule at random and choose the number of atoms that are to be regrown. With equal probability we regrow the atoms at the end or beginning of that part of the molecule that does not get regrown. We use the configurational-bias Monte Carlo technique for this move with acceptance rules

as given in Ref. 12. The number of trial orientations range from six for C_5 to ten for C_{48}. The total number of molecules was 200 for the short chain alkanes and 100 for the long chain alkanes.

During a volume change (4), we rescale the coordinates keeping the internal conformation of the molecule fixed. The maximum volume change is set such that 50% of the moves are accepted. For the exchange step (5), we have used the algorithm as described in the previous section. The number of trial orientations was equal to the number used for partial regrowing of a molecule.

Most simulations were started with equal initial densities of the two boxes. The initial density was chosen such that if at the given temperature the simulations would give coexisting liquid and gas densities equal to the experimental densities, the equilibrium volumes of the two boxes would be equal. Such an equilibrium configuration was subsequently used for some simulations at higher and lower temperatures. We found that systems could get easily trapped in undesired, far from equilibrium configurations when using initial densities which would yield widely differing gas and liquid volumes. Therefore, we used several systems with new initial densities during the determination of the entire coexistence curve. To generate the initial state, we placed the alkanes on a lattice. For long chain alkanes it was important to ''melt'' this lattice using ordinary N,V,T simulations before the Gibbs ensemble simulations were started. Immediately starting with the Gibbs ensemble simulations made the system initially move far away from equilibrium and subsequently very long simulations were required to reach equilibrium. For short chains, however, we could start directly with the Gibbs-ensemble simulations.

During the simulations the number of particles in the two boxes and the volumes of the boxes were stored. From these data we constructed a histogram of the densities and an $x-y$ plot.[4,30] At sufficiently low temperatures, the two boxes of the Gibbs ensemble do not change identity. Once one of the boxes contains the liquid phase it will keep it during the simulation. At these low temperatures, average densities in the two boxes are used as estimates of the coexistence densities. The accuracy is estimated using the standard block averaging techniques.[1] Close to the critical point the boxes may switch identity. At those conditions the density histograms are used and the coexistence densities are determined from the maxima of this density histogram. Estimates of the accuracy are made by dividing the simulations in blocks. The $x-y$ plots are used to judge the reliability of a simulation, for each sample two points are plotted on the $x-y$ plane $(x=n_1/N,\ y=V_1/V)$ and $(1-x,1-y)$. From these plots one can observe whether a simulation was reliable.[4]

The critical point was determined[36] by fitting the coexistence densities to the law of rectilinear diameters,[37]

$$\frac{\rho_l+\rho_g}{2}=\rho_c+A(T-T_c), \tag{21}$$

where $\rho_l(\rho_g)$ is the density of the liquid (gas) phase, ρ_c the critical density, and T_c the critical temperature. Furthermore, the results were also fitted to the scaling law for the density[38]

TABLE I. Comparison of nonbonded interaction parameters used to model alkanes. The energy parameter can be converted to (kJ/mol) by multiplication by 0.008 315.

	ϵ_{CH_3} (K)	ϵ_{CH_2} (K)	σ_{CH_3} Å	σ_{CH_2} Å	Ref.
C_5–C_{15}	90.5	49.3	3.94	3.94	8,25
C_{24} and C_{71}	49.3	49.3	3.94	3.94	25
C_5–C_8	104.0	49.7	3.923	3.923	42,43
C_{16}	50.5	50.5	4.045	4.045	79
C_5–C_8	102.0	51.3	3.983	3.863	42,43
decanoate	77.2	51.8	3.74	3.74	48
	90.5	55.3	3.86	3.98	80
C_5–C_8	96.0	56.7	4.123	3.723	42,43
C_5–C_8	116.0	56.8	3.70	3.70	42,43
C_{1000}	57.0	57.0	4.28	4.28	81
C_5–C_8	85.6	57.07	3.905	3.905	41
	88.1	59.4	3.905	3.905	19
C_5–C_8	88.1	59.38	3.820	3.820	41
C_{50}	60.1	60.1	3.80	3.80	82
C_5–C_8	92.0	65.5	4.323	3.523	42,43
C_4	72.0	72.0	3.923	3.923	18
C_4	84.0	84.0	3.923	3.923	17
C_4–C_{48}	114.0	47.0	3.93	3.93	this work

$$\rho_l-\rho_g=B(T-T_c)^{\beta}, \tag{22}$$

where β is the critical exponent. For small molecular fluids such as the Lennard-Jones fluid[5,30,39] the data can be fitted very well with an Ising-type critical exponent ($\beta=0.32$). For the short chain alkanes, C_5–C_{10}, we could fit the simulation data and experimental data well with such an Ising exponent, whereas a classical exponent ($\beta=0.5$) could not fit the data. For the long chain alkanes, the data were not sufficiently accurate to distinguish between the two exponents. To be consistent with the short chain lengths, we used the Ising exponent for all molecules. Note that this exponent is consistent with the experimental value for polymer solutions as determined by Dobashi *et al.*[40]

We tested our program by comparing our results with the Gibbs-ensemble simulations of an 8 bead Lennard-Jones polymer of Mooij *et al.*,[6] with which they were in excellent agreement. In addition, we compared our results with the simulation data reported by Laso *et al.*[8] The agreement was again very good. A more extensive discussion will be given in the next section.

IV. MODELS AND RESULTS

Over the last two decades various models to describe the interaction between alkanes have been developed. Table I shows the energy and size parameters of the models that use a Lennard-Jones potential for the nonbonded interactions. A comparison of the various models shows that for the size parameter the variation can be as much as 20%, although most models use a value of approximately 3.9 Å. For the energy parameters there is little consensus on the preferred values. Some models use the same value for ϵ for the methyl and methylene units while others use different ones. These differences can amount to a factor of 2.

These large differences in parameters motivated this study. The availability of techniques to determine the phase behavior of the alkanes over a large temperature range and for various chain lengths allows for an extensive comparison with experimental data.

In this study, we focus on united atom models. It is well known that united atom models fail to describe solid alkanes correctly.[26,27] Also for dense liquids Toxvaerd[21] observed that it is impossible to describe the equation of state of the alkanes consistently with a united atom model. Recently, Padilla and Toxvaerd[41] argued that it is even impossible to describe the second virial coefficient of the alkanes with such a model using realistic parameters. This observation is surprising since the assumptions underlying the united atom model should hold very well for alkanes in a low density gas phase. López Rodríguez *et al.*,[42,43] however, have shown that it is possible to describe the second virial coefficient accurately using a united atom model. It is therefore interesting to investigate how well a united atom model can describe vapor–liquid equilibria.

A. The OPLS model

1. The model

One of the most popular models used in simulations of alkanes and monolayers[44–46] is based on the OPLS model of Jorgensen *et al.*[19] This model has been further refined by Hautman and Klein[44] to include bond bending. The OPLS model uses a united atom description in which CH_2 and CH_3 groups are considered as one united atom. The nonbonded interactions between united atoms of different molecules and within a molecule (if two atoms are more than four atoms apart) are described with a truncated Lennard-Jones potential

$$u^{\mathrm{LJ}}(r_{ij}) = 4\epsilon_{ij}\left[\left(\frac{\sigma_{ij}}{r_{ij}}\right)^{12} - \left(\frac{\sigma_{ij}}{r_{ij}}\right)^{6}\right]. \tag{23}$$

The energy parameters of CH_2 and CH_3 groups are, respectively, $\epsilon_{CH_2} = 59.4$ (K) and $\epsilon_{CH_3} = 88.1$ (K). Throughout this work, we use $\epsilon_{ij} = \sqrt{\epsilon_i \epsilon_j}$ as the combining rule for the energy parameters of the unlike interactions. The size parameters of the methylene and methyl groups are assumed to be equal and have the value $\sigma = 3.905$ Å. The potential is truncated at 11.5 Å. No tail corrections have been applied. Note that tail corrections can have a significant effect on the phase diagram, for example, for the Lennard-Jones fluid including tail corrections this results in a critical temperature which is ~30% higher than without these corrections.[39] The intramolecular interactions consist of bond bending and torsion.[47] The distance between the atoms has been fixed to 1.53 Å. For the bond bending the van der Ploeg and Berendsen potential[48] is used

$$u^{\mathrm{bend}}(\theta) = \frac{1}{2} k_\theta (\theta - \theta_0)^2, \tag{24}$$

with $k_\theta = 62\,500$ (K rad^{-2}) and equilibrium angle $\theta_0 = 112$ (deg). For the torsion potential the original Ryckaert and Bellemans[17] potential is used

TABLE II. Results of the Gibbs-ensemble simulations for the *n*-alkanes as described with the OPLS model. T is the temperature, ρ_g, ρ_l are the densities of the gas and liquid phase, respectively, and "acc" is the probability of a successful exchange between the two boxes. The subscripts give the accuracy of the last decimal(s), i.e., 0.0815_{30} is 0.0815 ± 0.0030.

T (K)	ρ_g (g cm^{-3})	ρ_l (g cm^{-3})	acc (%)
	pentane C_5		
350	0.0077_9	0.57_1	0.5
402	0.026_1	0.51_1	2.2
435	0.059_5	0.47_1	4.1
450	0.07_2	0.43_4	8.1
460	0.08_2	0.39_3	9.2
470	0.10_1	0.36_2	10.7
	octane C_8		
424	0.003_3	0.620_7	0.2
464	0.008_3	0.581_5	0.8
488	0.014_7	0.54_1	1.5
512	0.013_7	0.545_{10}	1.8
536	0.024_{20}	0.51_2	3.0
560	0.043_7	0.475_{10}	5.1
576	0.055_{10}	0.42_2	5.8
584	0.08_2	0.43_2	6.5
592	0.09_2	0.40_2	8.9
596	0.11_4	0.35_5	12.3
	dodecane C_{12}		
550	0.006_2	0.615_2	0.4
600	0.010_2	0.570_3	1.4
625	0.020_{10}	0.55_1	1.4
650	0.024_6	0.505_{10}	3.1
665	0.048_{10}	0.49_2	3.4
680	0.05_2	0.465_{10}	4.0
700	0.085_{20}	0.445_{20}	5.5
	hexadecane C_{16}		
625	0.008_9	0.61_1	0.1
675	0.022_9	0.58_1	0.7
725	0.035_{10}	0.52_1	1.8
750	0.049_{10}	0.47_1	3.4
770	0.08_2	0.45_2	3.9
780	0.09_3	0.44_2	4.0
790	0.13_2	0.41_2	4.2

$$u^{\mathrm{tors}}(\phi) = \sum_{k=0}^{5} c_k \cos^k(\phi), \tag{25}$$

where ϕ is the dihedral angle. The parameters are $c_0 = 1116$ (K), $c_1 = 1462$ (K), $c_2 = -1578$ (K), $c_3 = -368$ (K), $c_4 = 3156$ (K), and $c_5 = -3788$ (K).

2. Results and discussion

For the OPLS model, we used the bond bending and the torsion potentials for the internal energy. In Appendix A, the details on how the trial orientations are generated are described.

The results of these simulations are shown in Table II. In Fig. 3 the vapor–liquid curve as obtained from the simulations using the OPLS model is compared with experimental data. This model has been fitted to the thermodynamic data of short chain alkanes at room temperature. Figure 3 shows that for pentane the agreement with experimental data is

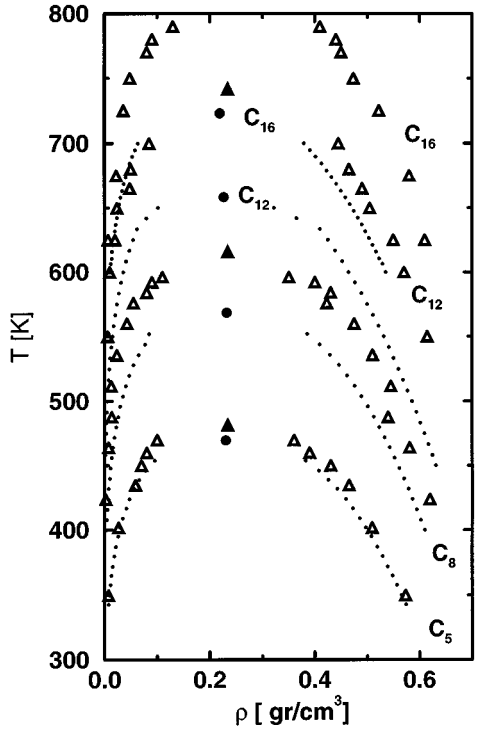

FIG. 3. Vapor–liquid equilibria of various alkanes as obtained from the Gibbs-ensemble simulations (open triangles) using the OPLS model. The small dots are experimental data (for C_5–C_9 the data are taken from Ref. 84 for larger chain lengths data are estimated from an equation of state). The large dots are the experimental critical points (Ref. 76). The filled triangle is the estimate of the critical point based on the simulation data.

excellent. For larger chain lengths the deviation from experimental data becomes significant. For hexadecane the coexistence curve is shifted approximately 100 (K). In Table III the estimated critical points are compared with the experimental values. For pentane the critical temperature is within 3% of the experimental value, for hexadecane the critical point is overestimated by 10%. Since the difference between the simulation results and the experimental data increases with chain length, a simple rescaling of the energy parameters is not expected to give a better description.

B. The de Pablo model

1. The model

Laso *et al.*[8] used the model introduced by de Pablo *et al.*[25] to calculate a coexistence point of several alkanes. The model of de Pablo also uses a Lennard-Jones potential to describe the nonbonded interactions between united atoms. The energy parameters are $\epsilon_{CH_2} = 49.3$ (K) and $\epsilon_{CH_3} = 90.5$ (K) and the size parameters have the same value for the methylene and methyl groups, namely $\sigma = 3.94$ Å. For the truncation of the potential the minimum image convention was used. The bond length was fixed at 1.53 Å and the bond angle was constrained to 112 deg. The Jorgensen torsion potential was used,

$$u^{\mathrm{tors}}(\phi) = c_0 + 0.5c_1(1+\cos\phi) + 0.5c_2(1-\cos 2\phi) + 0.5c_3(1+\cos 3\phi), \quad (26)$$

with $c_1 = 355$ (K), $c_2 = -68.19$ (K), and $c_3 = 791.3$ (K).

TABLE III. The critical points of the various models as calculated from the Gibbs-ensemble simulations. The experimental critical points are from Ref. 76 and the experimental critical pressures from Refs. 83,54. T_c is the critical temperature, ρ_c the critical density, and P_c the critical pressure. The subscripts give the accuracy of the last decimal(s).

	T_c (sim) (K)	T_c (exp) (K)	ρ_c (sim) (g cm^{-3})	ρ_c (exp) (g cm^{-3})	P_c (sim) (MPa)	P_c (exp) (MPa)
			OPLS model			
C_5	481_4	469.7	0.234_{10}	0.230		
C_8	616_5	568.6	0.234_8	0.232		
C_{12}	742_9	658.2	0.234_8	0.226		
C_{16}	808_6	723.0	0.254_{10}	0.219		
			Toxvaerd model			
C_5	439_3	469.7	0.225_8	0.230		
C_8	532_7	568.6	0.232_{13}	0.232		
C_{12}	592_3	658.2	0.205_{10}	0.226		
			de Pablo model			
C_8	584_{11}	568.6	0.221_{10}	0.232		
C_{24}	823_{14}	n.a.	0.219_{14}	n.a.		
			New model			
C_5	494_4	469.7	0.223_5	0.230	3.9_5	3.369
C_6	523_4	507.0	0.226_5	0.233	3.2_5	3.014
C_7	556_4	539.8	0.232_5	0.233	3.1_5	2.734
C_8	577_3	568.6	0.229_5	0.232	2.7_5	2.485
C_{10}	604_6	617.5	0.229_4	0.228	2.3_5	2.099
C_{12}	659_7	658.2	0.223_7	0.226	2.3_5	1.810
C_{16}	719_5	723.0	0.218_6	0.219	1.9_5	1.401
C_{24}	796_8	n.a.	0.205_9	n.a.	1.3_5	n.a.
C_{48}	924_{11}	n.a.	0.195_{14}	n.a.	1.0_6	n.a.

TABLE IV. Results of the Gibbs-ensemble simulations for the de Pablo model (see also the caption to Table II).

T (K)	ρ_g (g cm^{-3})	ρ_l (g cm^{-3})	acc (%)
	octane C_8		
473	0.017_5	0.53_1	0.8
498	0.021_5	0.505_1	2.6
523	0.04_1	0.46_1	4.7
548	0.06_2	0.42_2	7.1
563	0.08_2	0.38_4	14.3
	tetracosane C_{24}		
650	0.004_2	0.536_{10}	0.3
675	0.009_4	0.52_1	1.0
700	0.018_4	0.507_{10}	1.1
750	0.035_{10}	0.445_{10}	2.4
775	0.054_{10}	0.40_2	3.1

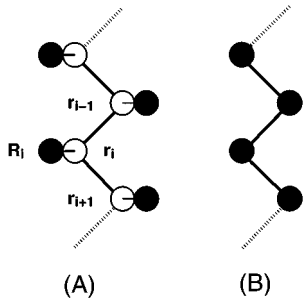

FIG. 4. Schematic sketch of Toxvaerd's model (a). The interaction sites of the nonbonded interactions (filled circles) are displaced (to the position of the valence electrons) with respected to the center of the carbons (open circles). (b) gives the approximated united atom model in which the interaction sites are at the same position as the center of the carbons.

2. Results and discussion

The vapor–liquid equilibrium densities as obtained from the model of de Pablo *et al.* are given in Table IV. Our data are in excellent agreement with those reported by Laso *et al.*[8] The estimated critical points are listed in Table III. The model proposed by de Pablo *et al.* gives a better overall description than the OPLS model (see Sec. IV A 2).

Laso *et al.* used a similar method to calculate the vapor–liquid curve. This method has been developed by de Pablo *et al.*[22] and is referred to as continuum-configurational-bias Monte Carlo. This method also combines the Gibbs-ensemble technique with the Rosenbluth algorithm to insert chain molecules. An important issue pointed out by Laso *et al.*[8] is that the continuum-configurational-bias Monte Carlo becomes computationally expensive for systems of pure alkanes of more than about twenty segments. Comparison of the acceptance probability of octane with the corresponding one of tetracosane (C_{24}) shows that in our version this probability does not decrease significantly. To see the reason for this, it is instructive to compare the two schemes in some detail.

The difference between our algorithm and the scheme proposed by de Pablo *et al.*[22] is the method in which the trial orientations are generated. In the model used by Laso *et al.*[8] the bond angle and bond length are fixed and therefore one has to generate only the torsional angle ϕ. De Pablo *et al.* generate the first torsional angle (ϕ_1) at random and the other $n-1$ angles are calculated from

$$\phi_{i+1}=\phi_i+2\pi/n.$$

Laso *et al.* used $n=12$ which gives twelve equally spaced trial orientations. Note that in the Rosenbluth factor of the de Pablo scheme the torsional potential has to be included.

To compare the efficiency of the scheme of de Pablo *et al.* and the scheme utilized in this work, we consider a model which has only internal interactions (i.e., only the torsional potential). For our algorithm this implies that there are no external interactions and hence the Rosenbluth factors of *all* generated conformations are by definition one. Therefore, all conformations that are generated will be accepted with probability one *irrespective* of the length of the molecule. In the scheme advocated by de Pablo *et al.*, however, the torsional potential appears in the Rosenbluth factor and hence in the acceptance rule. As a consequence, the probability of acceptance will be less than unity. Moreover, since the Rosenbluth factor is a product of the Boltzmann factors of the torsional potentials, this probability will decrease rapidly with chain length. For a system with external interactions, our scheme has the additional advantage that we only calculate the (expensive) external interactions for trial orientations that already have an "optimal" torsion potential. In the scheme of de Pablo *et al.*,[22] most trial orientations have such a high torsional potential that they have a very low probability of being accepted, yet for all these orientations the nonbonded interactions have to be calculated. These two factors make our scheme already an order of magnitude more efficient for C_{15} and up to several orders of magnitude for the longer chains. In addition, the approach of de Pablo *et al.* is very inefficient for potentials that are strongly peaked such as bond bending and bond vibration.

C. The Toxvaerd model

1. The model

Toxvaerd[21,49] introduced an anisotropic potential to model the effects of hydrogen on the thermodynamic properties without increasing the number of interaction sites. In this model, the interaction site of the nonbonded Lennard-Jones potential is displaced with respect to the center of mass of the carbon atoms (see Fig. 4),

$$u^{\mathrm{LJ}}(R_{ij})=4\epsilon_{ij}\left[\left(\frac{\sigma_{ij}}{R_{ij}}\right)^{12}-\left(\frac{\sigma_{ij}}{R_{ij}}\right)^{6}\right], \tag{27}$$

where R_{ij} is the distance between the interaction sites. The relation between $\mathbf{R}_i$ and the centre of mass $\mathbf{r}_i$ of atom i is given by

$$\mathbf{R}_i=\mathbf{r}_i+d\,\frac{\mathbf{r}_i-0.5(\mathbf{r}_{i+1}-\mathbf{r}_i)}{|\mathbf{r}_i-0.5(\mathbf{r}_{i+1}-\mathbf{r}_i)|}. \tag{28}$$

Padilla and Toxvaerd[49] use $d=0.37$ (Å) for the CH_2 groups and $d=0.275$ (Å) for the CH_3 groups. The parameters of the Lennard-Jones potential are $\epsilon_{CH_3}=120$ (K), $\epsilon_{CH_2}=80$ (K),

TABLE V. Results of the Gibbs-ensemble simulations for the Toxvaerd model (see also the caption to Table II).

T (K)	ρ_g (g cm^{-3})	ρ_l (g cm^{-3})	acc (%)
	pentane C_5		
300	0.005_1	0.608_5	0.1
325	0.008_2	0.580_5	0.3
350	0.012_3	0.54_1	0.9
375	0.028_5	0.51_2	1.5
400	0.047_{10}	0.45_2	3.5
410	0.063_{10}	0.43_1	4.5
420	0.07_2	0.39_2	7.6
430	0.09_2	0.34_2	10.5
	octane C_8		
425	0.015_5	0.555_{12}	0.4
450	0.027_{10}	0.525_{10}	0.8
475	0.047_{10}	0.49_1	1.4
500	0.050_{10}	0.425_{10}	5.1
520	0.09_2	0.35_1	9.6
	dodecane C_{12}		
450	0.004_3	0.61_1	0.03
475	0.011_5	0.580_6	0.06
500	0.010_5	0.532_7	0.3
525	0.015_6	0.49_2	0.6
550	0.029_8	0.45_2	1.5
575	0.045_{12}	0.38_2	6.0
590	0.16_7	0.28_3	7.0

and $\sigma_{CH_3}=\sigma_{CH_2}=3.527$ (Å). The potential is truncated at 12.0 (Å) and the usual tail corrections are applied.[1]

The intramolecular interactions include bond bending and torsion. For the bond bending Eq. (24) is used with $k_\theta=62\ 500$ (K) and $\theta_0=113.3$ deg. For the torsion, Eq. (25) was used with the parameters proposed by Padilla and Toxvaerd,[49] namely $c_0=1038$ (K), $c_1=2426$ (K), $c_2=81.6$ (K), $c_3=-3129$ (K), $c_4=-163$ (K), and $c_5=-252$ (K). The bond length was fixed to 1.539 (Å).[50]

2. Simulation details

The configurational-bias Monte Carlo scheme can not be applied directly to the Toxvaerd model because we have to know the position of atom $l+1$ to determine the position of the interaction site of atom l. We have used the following algorithm to make configurational-bias Monte Carlo simulations for this model possible.

Let us define an approximate potential, denoted by $\bar{u}$, which is identical to the Toxvaerd model but the interaction site of the nonbonded interaction is at the position of the carbon atoms. Hence the approximate model is an ordinary united-atom model (see Fig. 4) for which we can use the configurational-bias technique as described in Sec. II B. The probability of generating conformation n is given by

$$P(o\rightarrow n)=\frac{\exp[-\beta\bar{U}(n)]}{\bar{W}(n)}, \tag{29}$$

where $\bar{U}(n)=\Sigma_{i=1}^{M}\bar{u}_i$. The bar above the symbols indicate that this property is calculated with the approximate potential. The Rosenbluth factor is given by

$$\bar{W}(n)=\exp[-\beta\bar{u}_1(n)]\prod_{j=2}^{M}\sum_{i=1}^{k}\exp[-\beta\bar{u}_j(n_i)]. \tag{30}$$

In addition, we also calculate the difference in energy between the Toxvaerd potential and the approximate potential of the molecule in the *selected* conformation

$$\delta U(n)=U(n)-\bar{U}(n). \tag{31}$$

For the old conformation, we determine the Rosenbluth factor $\bar{W}(o)$ using the approximate potential and we calculate the energy difference between the two potentials of the old conformation

$$\delta U(o)=U(o)-\bar{U}(o). \tag{32}$$

If the move is the regrowing of part of a molecule, it is accepted with a probability

$$\mathrm{acc}(o\rightarrow n)=\min\left(1,\frac{\bar{W}(n)}{\bar{W}(o)}\exp\{-\beta[\delta U(n)-\delta U(o)]\}\right). \tag{33}$$

If the move involves an exchange of a molecule between the two boxes, the acceptance rule is

$$\mathrm{acc}(o\rightarrow n)=\min\left(1,\frac{V_1(N-n_1)}{(V-V_1)(n_1+1)}\frac{\bar{W}(n)}{\bar{W}(o)}\times\exp\{-\beta[\delta U(n)-\delta U(o)]\}\right). \tag{34}$$

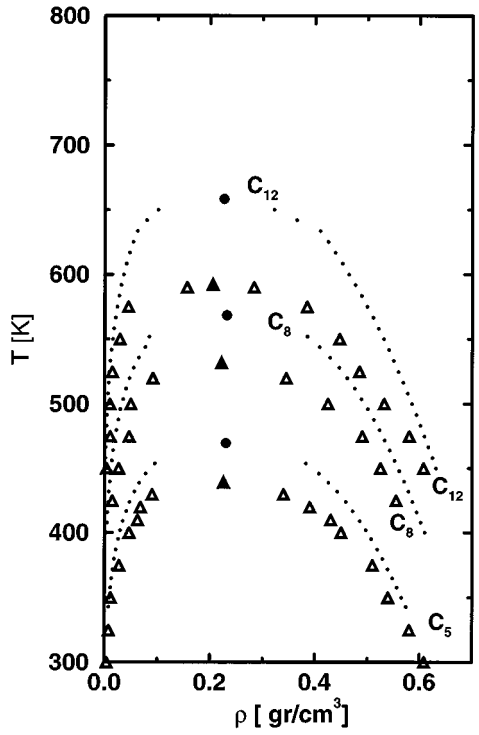

FIG. 5. Vapor–liquid equilibria of Toxvaerd's model (see also the caption to Fig. 3).

TABLE VI. Results of the Gibbs-ensemble simulations using the model presented in this work (see also the caption to Table II).

T (K)	ρ_g (g cm^{-3})	ρ_l (g cm^{-3})	acc (%)
	pentane C_5		
350	0.007_5	0.556_5	0.4
365	0.009_5	0.543_5	0.6
375	0.014_5	0.528_5	0.8
385	0.022_5	0.52_5	1.1
400	0.021_{15}	0.50_1	1.6
415	0.026_5	0.482_5	2.1
425	0.030_{10}	0.475_{10}	2.5
435	0.044_{10}	0.458_{10}	3.5
440	0.046_{10}	0.446_{10}	5.4
445	0.047_{10}	0.430_{10}	5.1
455	0.055_{10}	0.41_1	6.8
465	0.07_2	0.40_2	6.7
475	0.09_1	0.380_1	7.4
	hexane C_6		
350	0.003_2	0.596_5	0.1
375	0.008_3	0.577_7	0.2
385	0.009_3	0.565_7	0.3
400	0.010_5	0.544_{10}	0.6
415	0.017_5	0.527_5	1.0
425	0.017_5	0.515_5	1.3
450	0.028_5	0.48_1	2.7
465	0.042_5	0.464_5	3.2
475	0.050_5	0.443_5	5.1
500	0.07_3	0.39_3	7.3
	heptane C_7		
375	0.0042_{50}	0.605_5	0.1
385	0.0048_{50}	0.595_5	0.2
415	0.0087_{30}	0.560_3	0.4
425	0.011_3	0.551_5	0.6
435	0.014_3	0.543_4	0.8
450	0.021_3	0.531_{10}	1.1
475	0.033_3	0.497_4	2.1
490	0.041_7	0.479_7	2.9
500	0.046_{10}	0.462_7	4.0
515	0.060_5	0.432_5	5.3
	octane C_8		
400	0.004_1	0.605_3	0.1
425	0.007_5	0.585_7	0.2
435	0.008_5	0.573_7	0.8
450	0.012_5	0.552_7	1.0
460	0.013_3	0.545_4	1.0
475	0.015_5	0.526_7	2.2
485	0.028_3	0.521_4	1.4
490	0.027_5	0.517_7	1.8
503	0.035_5	0.491_7	2.9
510	0.033_3	0.468_5	3.5
523	0.047_5	0.457_7	4.7
535	0.052_5	0.439_8	5.8
550	0.08_1	0.40_1	6.8
	decane C_{10}		
425	0.002_2	0.620_{10}	0.1
450	0.005_2	0.595_{10}	0.2
475	0.010_2	0.574_{10}	0.6
500	0.014_5	0.531_{10}	1.5
515	0.018_5	0.511_{10}	2.3
530	0.030_5	0.499_{10}	2.5
550	0.048_7	0.454_{15}	4.7
575	0.07_1	0.425_{10}	5.8

TABLE VI. (*Continued*.)

T (K)	ρ_g (g cm^{-3})	ρ_l (g cm^{-3})	acc (%)
	dodecane C_{12}		
450	0.005_5	0.625_5	0.03
475	0.005_4	0.602_5	0.2
500	0.012_5	0.576_5	0.5
525	0.015_5	0.545_5	1.2
550	0.014_5	0.518_5	2.4
575	0.024_{10}	0.494_1	2.0
585	0.044_{10}	0.466_{10}	3.5
600	0.060_{10}	0.437_{20}	4.8
615	0.055_{10}	0.45_1	3.6
	hexadecane C_{16}		
550	0.0058_{10}	0.581_5	0.2
575	0.0056_{10}	0.55_1	0.9
600	0.014_5	0.526_{10}	1.0
615	0.022_5	0.514_{10}	1.5
625	0.02_1	0.518_{10}	1.2
640	0.030_5	0.483_{10}	2.4
650	0.033_5	0.477_{10}	2.2
660	0.022_{10}	0.44_2	4.8
675	0.047_5	0.423_7	6.1
685	0.06_1	0.396_{10}	6.5
	tetracosane C_{24}		
625	0.004_3	0.559_5	0.2
650	0.010_5	0.547_{10}	0.3
665	0.013_5	0.532_{10}	0.5
675	0.010_5	0.517_{10}	0.8
685	0.011_{10}	0.503_{10}	1.2
700	0.016_{10}	0.48_1	1.1
715	0.016_{10}	0.454_{15}	1.6
725	0.022_{10}	0.435_{15}	2.3
735	0.034_{10}	0.45_1	1.0
750	0.040_{10}	0.40_1	3.7
	octatetracontane C_{48}		
800	0.005_3	0.465_{10}	0.2
825	0.011_5	0.453_{10}	0.3
850	0.020_{10}	0.419_{10}	0.4
875	0.036_{10}	0.393_{15}	1.1
890	0.055_{20}	0.35_3	1.4
900	0.06_3	0.32_3	1.9

In Appendix B it is proven that this scheme indeed samples the desired distribution of configurations.

This method is similar to what can be used for systems with ''expensive'' potentials. In such a model one can grow the molecules with an approximate potential which is very ''cheap.'' The correct energy of the conformation, as given by the expensive potential, is only calculated once, namely for the selected conformation and not for every trial orientation.

3. Results

We have calculated the vapor–liquid curves of pentane, octane, and dodecane. The results are presented in Table V. The simulation results are compared with experimental data in Fig. 5. The critical points are given in Table III. For pentane Toxvaerd's model predicts the critical point at a much lower temperature than the experimental one. Note that although for small chain lengths results obtained with the

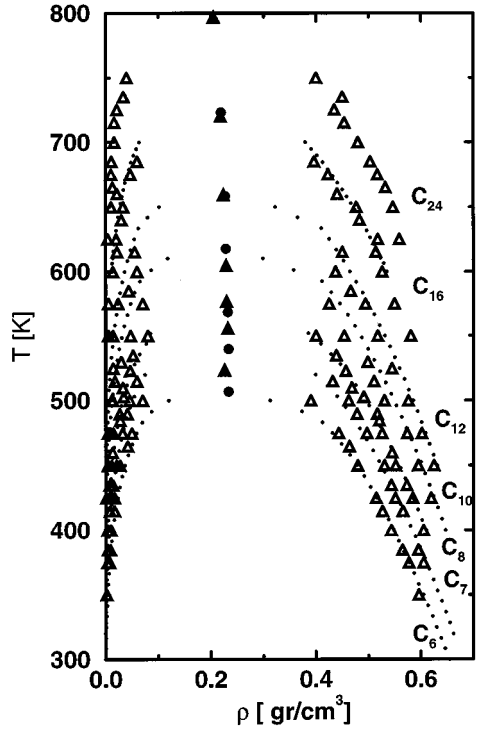

FIG. 6. Vapor–liquid equilibria of the model presented in this work (see also the caption to Fig. 3).

OPLS model agree better with experimental data than those obtained with Toxvaerd's model, the difference between experimental data and the predictions of Toxvaerd's model does not increase with chain length. This suggests that by rescaling of the parameters a better quantitative agreement may be obtained.

D. New model

Comparison of the parameters of the nonbonded interactions of the OPLS model with those used by de Pablo *et al.*[25] shows that in their study the ratio $\epsilon_{CH_3}/\epsilon_{CH_2}$ is much larger than the corresponding ratio for the OPLS model. Furthermore, the ϵ_{CH_2} has a much larger value in the OPLS than in the model of de Pablo *et al.* Since this parameter determines to a large extent the value of the critical temperature, it becomes clear why the OPLS model predicts a much higher critical point than the model of de Pablo *et al.* A similar set of parameters has been obtained by López Rodríguez *et al.*[42,43] from a study of the virial coefficients of alkanes. To describe these virial coefficients accurately López Rodríguez *et al.* had to introduce a low value of ϵ_{CH_2} and a large difference between ϵ_{CH_2} and ϵ_{CH_3}. We used the observations of López Rodríguez *et al.* and de Pablo *et al.* as a starting point in investigating whether a united-atom model can give a good description of a large range of alkanes. The model described below gave a good overall description of the phase behavior.

1. The model

The nonbonded interactions between the united atoms are described with a Lennard-Jones potential where the energy parameters are $\epsilon_{CH_2} = 47.0$ (K) and $\epsilon_{CH_3} = 114$ (K). The size parameters have the same value for the methylene and methyl groups, namely $\sigma = 3.93$ Å. The potential was truncated at 13.8 Å and the usual tail corrections were applied.

The bond-bending potential[48] is of the form of Eq. (24) with $k_\theta = 62\,500$ (K rad^{-2}) and equilibrium angle $\theta_0 = 114$ deg. The torsion potential[19] is of the form of Eq. (26) with parameters $c_1 = 355$ (K), $c_2 = -68.19$ (K), and $c_3 = 791.3$ (K). We also tested the Ryckaert and Bellemans torsion potential (25), but no significant differences in the phase behavior could be observed.

2. Results and discussion

In Table VI, the results of the simulations are summarized. In Fig. 6, the results of the simulations are compared with data for the *n*-alkanes for which either experimental data are available or can at least be estimated with some reliability (C_5–C_{16}), the overall agreement with experimental data is surprisingly good. In Table III the estimated critical properties are listed. This table shows that for pentane the critical temperature is slightly overestimated.

These results show that it is possible to model the phase behavior of the *n*-alkanes over a large temperature range with a united atom model. The density appears to be sufficiently low so that it is not necessary to model the hydrogens explicitly. To obtain this agreement, a large difference between the energy parameters of the CH_2 interactions and the CH_3 interaction was required. Similar conclusions have been obtained by López Rodríguez *et al.*,[42,43] Almarza *et al.*,[51] and de Pablo and co-workers.[8,25] Padilla and Toxvaerd,[41] however, argued that a ratio of $\epsilon_{CH_3}/\epsilon_{CH_2}$ that is much larger than 1.5 is unphysical. López Rodríguez *et al.*[42,43] showed that a high ratio of $\epsilon_{CH_3}/\epsilon_{CH_2}$ is to some extent due to the assumption $\sigma_{CH_3} = \sigma_{CH_2}$. If σ_{CH_3} is taken as larger than σ_{CH_2}, the ratio $\epsilon_{CH_3}/\epsilon_{CH_2}$ would not be as large. It would be interesting to investigate this in further detail.

V. CRITICAL PROPERTIES OF THE ALKANES

Alkanes are thermally unstable above approximately 650 (K), which makes experimental determination of the critical points of alkanes longer than decane (C_{10}) extremely difficult. Long alkanes, however, are present in mixtures of practical importance for the petrochemical industry. In these mixtures, the number of components can be so large that it is not practical to determine all phase diagrams experimentally. One therefore has to rely on predictions made by equations of state. The parameters of these equations of state are directly related to the critical properties of the pure components. Therefore, the critical properties of the long-chain alkanes are essential in the design of petrochemical processes, even if they are unstable close to the critical point. However, as experimental data are scarce and contradictory, we had to rely on semiempirical methods to estimate the critical properties.[52–55]

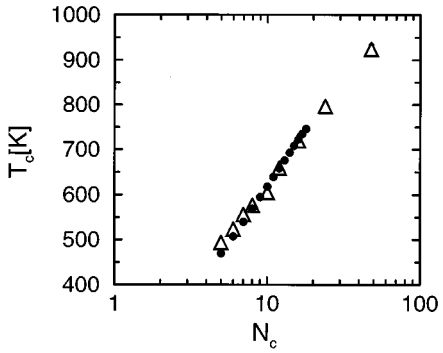

FIG. 7. Critical temperature T_c as a function of carbon number N_c. △, the simulation data and ●, the experimental data from Refs. 76,55.

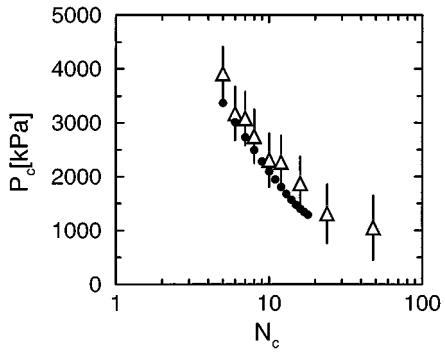

FIG. 9. Critical pressure P_c as a function of carbon number N_c. △, the simulation data and ●, the experimental data from Refs. 83,54.

More than 40 years ago, the critical properties and the equation of state of *n*-alkanes were already the topic of theoretical investigations. Most of these studies were aimed at establishing empirical relationships between the critical properties and carbon number[56–62] based on the compilation of the available experimental data by Egloff.[63] A more fundamental approach was taken by Prigogine and co-workers,[64–66] who extended the cell method to *n*-mers to derive an equation of state for these components. Hijmans[67] used the results of Prigogine and co-workers to derive phenomenological relations for the chain length dependence of the thermodynamic properties. Prigogine's treatment of *r*-mers predicts that the critical temperature scales as $T_c \propto n/(n^{1/2}+1)^2$ and the critical density as $\rho_c \propto n^{-1/2}$, where n is the number of monomeric units in the chain.

Kurata and Isida[68] assumed the vapor–liquid equilibria to be identical to a solution of rodlike polymers in a solvent of small molecules. The chain length dependence of the critical properties of the *n*-alkanes is, with this assumption, identical to the dependence of a polymer solution. Interestingly, the Flory–Huggins theory[69–72] for polymer solutions also predicts that the critical density *decreases* with chain length, i.e., $\rho_c \propto n^{-1/2}$.

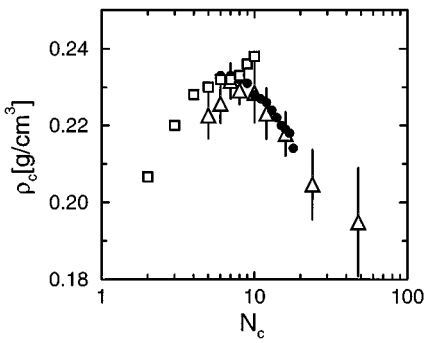

FIG. 8. Critical density ρ_c as a function of carbon number N_c. △, the simulation data and ●, the experimental data from Anselme *et al.* (Ref. 76) and □, the data of Steele (as published in Ref. 55).

The experimental data available to Kurata and Isida showed that the critical density was *independent* of chain length, suggesting that both the theory of Prigogine and of Flory–Huggins were not directly applicable to these systems. To take into account this experimental fact, Kurata and Isida made an ad hoc assumption on the scaling behavior of the critical properties such that $\rho_c \propto n^{1/3}/(n^{1/3}+1)$. Kreglewski and Zwolinski,[73] Nakanishi *et al.*,[74] and more recently Tsonopoulos[52] used Kurata and Isida's empirical corrections of the Flory scaling relations to correlate the various critical properties successfully.

Prigogine's treatment of *r*-mers was later revisited by Flory, Orwoll, and Vrij,[75] this study showed that the lattice treatment inherent in the cell theory (which by fixing the nearest neighbors of a given molecule exactly at their mean separation, suppresses the randomness which is the foremost characteristic of the liquid state). Flory and co-workers[75] then continued and derived a continuum theory. This theory was recently used by Tsonopoulos and Tan[55] to describe the more recent experimental data successfully.

Experimentally, the critical properties of *n*-alkanes up to C_{18} have been studied by Anselme *et al.*[76] (see Figs. 7 and 8). The most often used extrapolations assume that the critical density is a monotonically increasing function of the carbon number, approaching a limiting value for the very long alkanes.[52,55] In contrast to the expectations which are based on these extrapolations, the experimental data of Anselme *et al.*[76] indicate that the critical density has a maximum for C_8 and then *decreases* monotonically. The experimental data of Steele (as reported in by Tsonopoulos and Tan[55]), however, do not provide any evidence for such a maximum (see Fig. 8).

Since we can use our simulation technique to study phase behavior of the longer alkanes at conditions where experiments are not (yet) feasible, we are in a position to make predictions of the critical properties of these molecules. Figure 7 shows that our calculations of the critical temperatures are in very good agreement with both the data of Steele and Anselme *et al.* The simulation results for the critical densities (Fig. 8) show the same trend as observed by Anselme *et al.* and therefore strongly support these experiments. At this point it is interesting to note that Mooij *et al.*[6]

and Sheng *et al.*[77] used Monte Carlo simulations to study the vapor–liquid curve of a polymeric bead-spring model for various chain lengths. These studies also show a decrease of the critical density as a function of chain length. This indicates that the decrease of the critical density with chain length is a more general feature of chain molecules that does not depend on the details of a particular model.

The results for the critical pressure are presented in Table III. The critical pressure was calculated from fitting the vapor pressure data of the simulations to the Clausius–Clapeyron equation. This equation was then used to extrapolate to the critical point. Comparison with the experimental data (see Fig. 9) shows that, considering the accuracy of the data, the agreement between the simulations and experiments is very good.

VI. CONCLUDING REMARKS

In this work we have used the Gibbs-ensemble technique in combination with the configurational-bias Monte Carlo method to determine the vapor–liquid curves of various *n*-alkanes. Different alkane models have been compared and a new model is introduced that can describe the vapor–liquid curve over a large temperature range for a large number of alkanes.

Whereas the conventional Gibbs-ensemble technique is limited to butane or pentane, the combination with configurational-bias Monte Carlo allows for the simulation of chains as long as C_{48}. On an IBM/340 workstation such a simulation takes approximately 1 week of cpu time, for octane (C_8) the corresponding cpu time is approximately 12 h. Note that the increase of cpu time for the long chain alkanes is mostly due to the increase of the number of atoms (for C_{48} we use ~5000 atoms and for C_8 ~1000). Since the probability of a successful exchange between the liquid and vapor phase does not lessen significantly in our scheme, we expect that it is possible to determine the coexistence curve of even longer chains.

This work demonstrates that for modeling vapor–liquid coexistence a relatively simple united-atom model is sufficient to obtain a very good agreement with experimental data and it is not necessary to take the hydrogen atoms explicitly into account. To get this agreement it was necessary to make the energy parameters of the nonbonded potential of the CH_3–CH_3 interaction very different from the corresponding value for the CH_2–CH_2 interaction. This observation is in agreement with the conclusions of other simulation studies.[8,25,42,51]

For petrochemical applications knowledge of the critical properties of the *n*-alkanes is of interest even at temperatures where these molecules are thermally unstable. Even qualitative aspects, such as the chain-length dependence of the critical properties, are poorly understood for these systems. Our calculations show that, in contrast to the traditional view, the critical density of the long alkanes decreases rather than increases with carbon number. The simulations presented in this work show that it is possible to use simulations as an ''engineering tool'' to generate reliable data for the critical properties of the *n*-alkanes at conditions where experiments are not (yet) feasible.

ACKNOWLEDGMENTS

We would like to thank M. J. Anselme, D. Frenkel, W. G. Heitman, A. K. van Helden, H. P. C. E. Kuipers, J.-P. Ryckaert, S. Schreuder, and M. Sprik for their contributions to this work.

APPENDIX A: GENERATION OF TRIAL ORIENTATIONS

In this Appendix, we demonstrate the way we generate the trial orientations in the configurational-bias Monte Carlo scheme.

Let us first consider the general case with flexible bond length, bond bending, and torsion. The probability that we generate a trial configuration **b** is given by

$$P(\mathbf{b})d\mathbf{b}=\frac{\exp[-\beta u^{\mathrm{int}}(\mathbf{b})]d\mathbf{b}}{C}, \tag{A1}$$

where C is a normalization constant which is defined by

$$C\equiv\int_{\mathbf{b}} d\mathbf{b}\ \exp[-\beta u^{\mathrm{int}}(\mathbf{b})]. \tag{A2}$$

Note that in the configurational-bias Monte Carlo scheme we do not have to calculate this constant.

It is convenient to represent the position of a atom using the bond length r, bond angle θ, and torsional angle ϕ (see Fig. 10). With these coordinates the volume element $d\mathbf{b}$ is given by

$$d\mathbf{b}=r^2\ \cos(\theta)dr\,d\theta\,d\phi. \tag{A3}$$

The internal energy is the sum of the bond vibration potential, the bond-bending potential, and the torsion potential,

$$u^{\mathrm{int}}(r,\theta,\phi)=u_{\mathrm{vib}}(r)+u_{\mathrm{bend}}(\theta)+u_{\mathrm{tors}}(\phi). \tag{A4}$$

Substitution of Eqs. (A4) and (A3) into Eq. (A1) gives

$$\begin{aligned}P(\mathbf{b})d\mathbf{b}&=P(r,\theta,\phi)r^2dr\,d\theta\,d\phi\\&=\exp[-\beta u_{\text{bond-vib}}(r)]r^2dr\\&\quad\times\exp[-\beta u_{\mathrm{bend}}(\theta)]\cos(\theta)d\theta\\&\quad\times\exp[-\beta_{\mathrm{tors}}(\phi)]d\phi.\end{aligned} \tag{A5}$$

In our simulations we have used an alkane model with fixed bond length, therefore in our case the first term in Eq. (A5) is a constant.

For the second carbon atom there are no internal interactions other than the constraints of the bond length. The distribution of trial orientations, Eq. (7) reduces to

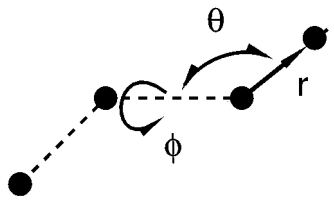

FIG. 10. Definition of the bond length r, bond angle θ, and torsional angle ϕ.

$$P_2(\mathbf{b})d\mathbf{b} \propto \cos(\theta)d\theta d\phi. \tag{A6}$$

Hence, the trial orientations are randomly distributed on the surface of a sphere. The algorithm that we have used for generating random vectors on the surface of a sphere is described in Ref. 1.

For the third atom, the internal energy contains the bond-bending energy as well. This gives for the distribution of trial orientations

$$P_3(\mathbf{b})d\mathbf{b} \propto \exp[-\beta u_{\text{bend}}(\theta)]\cos(\theta)d\theta d\phi. \tag{A7}$$

To generate k trial orientations that are distributed according to Eq. (7) we generate again a random vector on a unit sphere and determine the angle θ. This vector is accepted with a probability $\exp[-\beta u_{\text{bend}}(\theta)]$. If rejected, this procedure is repeated until a value of θ has been accepted. In Ref. 78 it is shown that this acceptance/rejection method indeed gives a distribution of trial orientations given by Eq. (7). Note that the term $\cos\theta$ is taken into account by generating a random vector on a sphere. In this way, k (or $k-1$ for the case of the old conformation) trial orientations are generated.

An alternative scheme would be to generate angle θ uniformly ($\in[0,\pi]$) and the bond-bending energy corresponding to this angle is calculated. This angle θ is accepted with a probability $\cos(\theta)\exp[-\beta u_{\text{bend}}(\theta)]$. If rejected, this procedure is repeated until a value of θ has been accepted. The selected value of θ is supplemented with a randomly selected angle ϕ. These two angles determine a new trial orientation.

For the fourth and higher carbon atoms, the internal energy includes both bond-bending and torsion energy. This gives for Eq. (7),

$$p_l^{\text{int}}(\mathbf{b})d\mathbf{b} \propto \exp[-\beta u_{\text{bend}}(\theta)] \times \exp[-\beta u_{\text{tors}}(\phi)]\cos(\theta)d\theta d\phi. \tag{A8}$$

We again generate a random vector on a sphere and calculate the bond-bending angle θ and torsion ϕ. These angles are accepted with a probability $\exp\{-\beta[u_{\text{bend}}(\theta)+u_{\text{tors}}(\phi)]\}$. If these angles are rejected, a new vectors are generated until one gets accepted.

Again the alternative scheme would be first to determine a bond-bending angle θ by generating θ uniformly on $[0,\pi]$ and calculating the bond-bending energy corresponding to this angle. This angle θ is then accepted with a probability $\cos(\theta)\exp[-\beta u_{\text{bend}}(\theta)]$. This procedure is continued until we have accepted an angle. Next generate a torsion angle randomly on $[0,2\pi]$ and accept this angle with a probability $\exp[-\beta u_{\text{tors}}(\phi)]$, again repeating this until a value has been accepted. In this scheme the bond angle and torsion are generated independently which can be an advantage in cases where the corresponding potentials are sharply peaked.

In the de Pablo model the bond angle is fixed. For the generation of the trial orientations this implies that Eqs. (A7) and (A8) must be replaced by an algorithm that generates orientations on the surface of a cone. The approximated potentials for Toxvaerd's model and the model introduced in this work are of the same form as the Jorgensen potential.

APPENDIX B: PROOF OF ALGORITHM FOR TOXVAERD'S POTENTIAL

In this Appendix we prove that the algorithm of Sec. IV C 2 for the Toxvaerd potential gives the desired distribution of configurations. The flow of configurations from state o to state n is given by

$$K(o\to n) = \mathcal{N}(o)\times p(o\to n)\times \text{acc}(o\to n). \tag{B1}$$

Imposing detailed balance and substitution of Eqs. (29) and (30) gives as condition for the acceptance rule

$$\begin{aligned}\frac{\text{acc}(o\to n)}{\text{acc}(n\to o)} &= \frac{\exp[-\beta U(n)]}{\exp[-\beta U(o)]} \\ &\quad\times \frac{\exp[-\beta \bar{U}(n)]}{\bar{W}(n)}\frac{\bar{W}(o)}{\exp[-\beta \bar{U}(o)]} \\ &= \frac{\bar{W}(n)}{\bar{W}(o)}\exp\{-\beta[\delta U(n)-\delta U(o)]\}.\end{aligned} \tag{B2}$$

Acceptance rule (33) obeys this condition which proves that the correct distribution is sampled.

[1] M. P. Allen and D. J. Tildesley, *Computer Simulation of Liquids* (Clarendon, Oxford, 1987).
[2] A. Z. Panagiotopoulos, Mol. Phys. **61**, 813 (1987).
[3] A. Z. Panagiotopoulos, N. Quirke, M. Stapleton, and D. J. Tildesley, Mol. Phys. **63**, 527 (1988).
[4] B. Smit, Ph. de Smedt, and D. Frenkel, Mol. Phys. **68**, 931 (1989).
[5] A. Z. Panagiotopoulos, Mol. Simul. **9**, 1 (1992).
[6] G. C. A. M. Mooij, D. Frenkel, and B. Smit, J. Phys. Condensed Matter **4**, L255 (1992).
[7] G. C. A. M. Mooij, Ph.D. thesis, Rijksuniversiteit Utrecht, The Netherlands, 1993.
[8] M. Laso, J. J. de Pablo, and U. W. Suter, J. Chem. Phys. **97**, 2817 (1992).
[9] J. Harris and S. A. Rice, J. Chem. Phys. **88**, 1298 (1988).
[10] J. I. Siepmann and D. Frenkel, Mol. Phys. **75**, 59 (1992).
[11] J. J. de Pablo, M. Bonnin, and J. M. Prausnitz, Fluid Phase Equil. **73**, 187 (1992).
[12] D. Frenkel, G. C. A. M. Mooij, and B. Smit, J. Phys. Condensed Matter **4**, 3053 (1992).
[13] R. F. Cracknell, D. Nicholson, N. G. Parsonage, and H. Evans, Mol. Phys. **71**, 931 (1990).
[14] J. I. Siepmann, S. Karaborni, and B. Smit, J. Am. Chem. Soc. **115**, 6454 (1993).
[15] J. I. Siepmann, S. Karaborni, and B. Smit, Nature **365**, 330 (1993).
[16] D. E. Williams, J. Chem. Phys. **47**, 4680 (1967).
[17] J. P. Ryckaert and A. Bellemans, Chem. Phys. Lett. **30**, 123 (1975).
[18] J. P. Ryckaert and A. Bellemans, Faraday Discuss. Chem. Soc. **66**, 95 (1978).
[19] W. L. Jorgensen, J. D. Madura, and C. J. Swenson, J. Am. Chem. Soc. **106**, 6638 (1984).
[20] W. L. Jorgensen and J. Tirado-Rives, J. Am. Chem. Soc. **110**, 1657 (1988).
[21] S. Toxvaerd, J. Chem. Phys. **93**, 4290 (1990).
[22] J. J. de Pablo, M. Laso, and U. W. Suter, J. Chem. Phys. **96**, 2395 (1992).
[23] P. M. Rodger, Mol. Phys. **76**, 1385 (1992).
[24] A. Berker, S. Chynoweth, U. C. Klomp, and Y. Michopoulos, J. Chem. Soc. Faraday Trans. **88**, 1719 (1992).
[25] J. J. de Pablo, M. Laso, J. I. Siepmann, and U. W. Suter, Mol. Phys. **80**, 55 (1993).
[26] J. P. Ryckaert and M. L. Klein, J. Chem. Phys. **85**, 1613 (1986).
[27] J. P. Ryckaert, M. L. Klein, and I. R. McDonald, Phys. Rev. Lett. **58**, 698 (1987).
[28] M. A. Moller, D. J. Tildesley, K. S. Kim, and N. Quirke, J. Chem. Phys. **94**, 8390 (1991).
[29] S. Karaborni and S. Toxvaerd, J. Chem. Phys. **96**, 5505 (1992).
[30] B. Smit, in *Computer Simulation in Chemical Physics*, NATO ASI, edited by M. P. Allen and D. J. Tildesley (Kluwer, Dordrecht, 1993), pp. 173–209.
[31] J. I. Siepmann, in *Computer Simulation of Biomolecular Systems: Theo-*

retical and Experimental Applications, edited by W. F. van Gunsteren, P. K. Weiner, and A. J. Wilkinson (Escom Science, Leiden, 1993), pp. 249–264.
[32] D. Frenkel, in *Computer Modelling of Fluids, Polymers and Solids*, NATO ASI, edited by C. R. A. Catlow (Kluwer, Dordrecht, 1990).
[33] B. Smit, Ph.D. thesis, Rijksuniversiteit Utrecht, The Netherlands, 1990.
[34] D. Frenkel, in *Computer Simulation in Chemical Physics*, NATO ASI, edited by M. P. Allen and D. J. Tildesley (Kluwer, Dordrecht, 1993), pp. 93–152.
[35] B. Smit and D. Frenkel, J. Chem. Phys. **94**, 5663 (1991).
[36] B. Smit and C. P. Williams, J. Phys. Condensed Matter **2**, 4281 (1990).
[37] J. S. Rowlinson and F. L. Swinton, *Liquids and Liquid Mixtures*, 3rd ed. (Butterworth, London, 1982).
[38] J. S. Rowlinson and B. Widom, *Molecular Theory of Capillarity* (Clarendon, Oxford, 1982).
[39] B. Smit, J. Chem. Phys. **96**, 8639 (1992).
[40] T. Dobashi, M. Nakata, and M. Kaneko, J. Chem. Phys. **72**, 6685 (1980).
[41] P. Padilla and S. Toxvaerd, Mol. Phys. **75**, 1143 (1992).
[42] A. López Rodríguez, C. Vega, J. J. Freire, and S. Lago, Mol. Phys. **73**, 691 (1991).
[43] A. López Rodríguez, C. Vega, J. J. Freire, and S. Lago, Mol. Phys. **80**, 1565 (1993).
[44] J. Hautman and M. L. Klein, J. Chem. Phys. **91**, 4994 (1989).
[45] J. I. Siepmann and I. R. McDonald, Phys. Rev. Lett. **70**, 453 (1993).
[46] J. I. Siepmann and I. R. McDonald, Mol. Phys. **79**, 457 (1993).
[47] Note that the model which is studied in this work includes bond bending potentials and has a slightly different potential for the torsion than that in the original work of Jorgensen *et al.* (Ref. 19). We found that the phase behavior is mainly determined by the nonbonded potential and is not very sensitive to the details of the intramolecular potentials. It can therefore be expected that differences between the model used in this work and the original alkane model of Jorgensen *et al.* are very small.
[48] P. Van der Ploeg and H. J. C. Berendsen, J. Chem. Phys. **76**, 3271 (1982).
[49] P. Padilla and S. Toxvaerd, J. Chem. Phys. **94**, 5650 (1991).
[50] Toxvaerd uses a slightly different bond-bending potential with equilibrium angles that depend on the molecule. Furthermore, in Toxvaerd's original model the bond length depends on chain length. These differences should have little effect on the phase behavior.
[51] N. G. Almarza, E. Enciso, and F. J. Bermejo, J. Chem. Phys. **96**, 4625 (1992).
[52] C. Tsonopoulos, AIChE J. **33**, 2080 (1987).
[53] K. Magoulas and D. Tassios, Fluid Phase Equilibria **56**, 119 (1990).
[54] A. S. Teja, R. J. Lee, D. Rosenthal, and M. Anselme, Fluid Phase Equilibria **56**, 153 (1990).
[55] C. Tsonopoulos and Z. Tan, Fluid Phase Equilibria **83**, 127 (1993).
[56] L. Grunberg and A. H. Nissan, Nature **161**, 170 (1948).
[57] L. Grunberg and A. H. Nissan, Trans. Faraday Soc. **44**, 1013 (1948).
[58] S. S. Mitra, J. Chem. Phys. **21**, 2234 (1953).
[59] Y. P. Varshi, J. Chem. Phys. **21**, 1400 (1953).
[60] L. Grunberg, J. Chem. Phys. **22**, 157 (1954).
[61] Y. P. Varshi, J. Chem. Phys. **22**, 150 (1953).
[62] Y. P. Varshi and S. N. Srivastava, J. Chem. Phys. **22**, 349 (1954).
[63] G. Egloff, *Physical Constants of Hydrocarbons* (Reinhold, New York, 1939).
[64] I. Prigogine, N. Trappeniers, and V. Mathot, J. Chem. Phys. **21**, 559 (1953).
[65] I. Prigogine, N. Trappeniers, and V. Mathot, Discuss. Faraday Soc. **15**, 93 (1953).
[66] I. Prigogine, *The Molecular Theory of Solutions* (Interscience, New York, 1957).
[67] J. Hijmans, Physica **27**, 433 (1960).
[68] M. Kurata and S. Isida, J. Chem. Phys. **23**, 1126 (1955).
[69] P. J. Flory, J. Chem. Phys. **10**, 51 (1942).
[70] P. J. Flory, J. Chem. Phys. **12**, 425 (1944).
[71] M. L. Huggins, Am. Chem. Soc. **64**, 1712 (1942).
[72] M. L. Huggins, J. Phys. Chem. **46**, 151 (1942).
[73] A. Kreglewski and B. J. Zwolinski, J. Phys. Chem. **65**, 1050 (1961).
[74] K. Nakanishi, M. Kurata, and M. Tamura, J. Chem. Eng. Data **5**, 210 (1960).
[75] P. J. Flory, R. A. Orwoll, and A. Vrij, J. Am. Chem. Soc. **86**, 3507 (1964).
[76] M. J. Anselme, M. Gude, and A. S. Teja, Fluid Phase Equilibria **57**, 317 (1990).
[77] Y.-J. Sheng, A. Z. Panagiotopoulos, S. K. Kumar, and I. Szleifer, Macromolecules **27**, 400 (1994).
[78] W. H. Press, B. P. Flannery, S. A. Teukolsky, and W. T. Vetterling, *Numerical Recipes: The Art of Scientific Computing* (Cambridge University, Cambridge, 1986).
[79] S. Chynoweth and Y. Michopoulos, Mol. Phys. **81**, 133 (1994).
[80] W. L. Jorgensen, J. Am. Chem. Soc. **103**, 335 (1981).
[81] D. Brown and J. H. R. Clarke, Macromolecules **24**, 2075 (1991).
[82] D. Rigby and R.-J. Roe, J. Chem. Phys. **87**, 7285 (1987).
[83] D. J. Rosenthal and A. S. Teja, AIChE J. **35**, 1829 (1989).
[84] B. D. Smith and R. Srivastava, *Thermodynamics Data for Pure Compounds: Part A Hydrocarbons and Ketones* (Elsevier, Amsterdam, 1986).